Transonic Shock Wave - Boundary Layer Interaction at a Convex Wall

B. Koren and W.J. Bannink

Laboratory for High Speed Aerodynamics
Department of Aerospace Engineering
Delft University of Technology
Kluyverweg 1
2629 HS Delft, The Netherlands

Delft Progr. Rep. 9 (1984) pp. 155-169
Received: August 1984

A standard finite element procedure has been applied to the problem of transonic shock wave - boundary layer interaction at a convex wall. The method is based on the analytical Bohning-Zierep model [1], where the boundary layer is perturbed by a weak normal shock wave which shows a singular pressure gradient at the curved edge of the boundary layer. In the present numerical method the application of a power law velocity distribution at the upstream end of the boundary layer has been abandoned and a more realistic distribution is applied. The results are compared to other numerical solutions and to experimental results. The differences are discussed together with the limitations introduced by the method.

1. Introduction

The problem of transonic shock wave - boundary layer interaction has been treated analytically by Bohning and Zierep [1]. They based their flow model on the experimental investigations of Ackeret, Feldmann and Rott [2] who studied the interaction of a normal shock with the boundary layer at a curved wall. The experiments indicated a very strong pressure gradient immediately downstream of the shock, manifesting itself in an expansion at the outer edge of the turbulent boundary layer. This rather pronounced expansion decreased when approaching the wall and it also induced an upstream effect in the boundary layer.

The after-expansion is also observed in the inviscid case at the downstream foot of a normal shock at a curved surface, a problem solved by Oswatitsch and

Zierep [3]. They found that at a convex wall the normal shock wave curves upstream, whereas at the foot the curvature is logarithmically infinite. As a consequence the velocity and the pressure gradient show a logarithmic singularity resulting in an expansion immediately downstream of the shock. Inspired by the similarity between the experimental results [2] and the inviscid solution [3] Bohning and Zierep [1] developed an analytical method that introduced the Oswatitsch-Zierep singularity into a viscous model. The numerical method described in the present paper is entirely based on the Bohning-Zierep model. Whereas Bohning and Zierep only could select a special initial velocity profile of the boundary layer (a profile that nevertheless is rather realistic) a computational approach might generalize the problem without more complexity.

2. The flow model

General description

The interaction region is considered [1] to extend over a distance 2ℓ upstream and downstream of the shock wave (Fig. 1), ℓ is of the order of the boundary layer thickness.

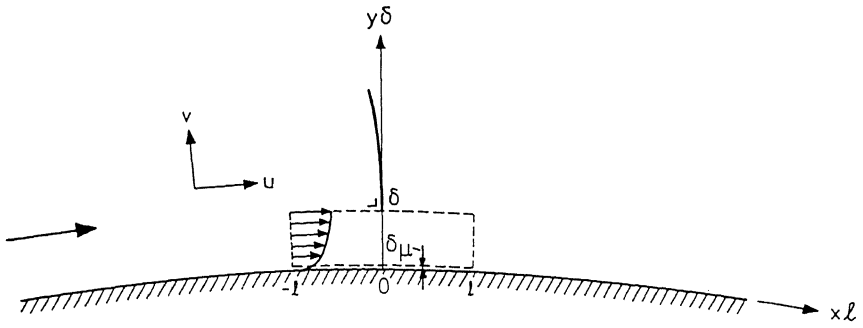

Fig.1: Region of interaction in the Bohning - Zierep model.

At the upstream end a boundary layer of the basic flow enters the region with a prescribed velocity profile; the thickness of the layer up to the level where the velocity is sonic is δ. The basic flow is considered to be independent of the distance along the wall (wall curvature $\ll 1$). The weak shock stands on the interaction region of thickness δ. The region is divided into two layers: a thick inviscid upper layer and a thin viscous sublayer with

thickness δ_μ.
The flow is composed of the above mentioned basic flow and a perturbation flow. The basic flow, which is known, remains when the shock strength vanishes and, therefore, the perturbation flow to be determined, exists only due to the shock wave. The perturbation quantities are considered small with respect to the basic flow quantities.

Boundary value problem

According to [1] a cartesian coordinate system is introduced (Fig. 1). The perturbation equations for the inviscid upper layer may be written as

$$\rho_o \frac{\partial u'}{\partial x} + M_o^* \frac{\partial \rho'}{\partial x} + \frac{\ell}{\delta} \frac{\partial(\rho_o v')}{\partial y} = 0 \tag{1}$$

for the continuity equation,

$$\rho_o M_o^* \frac{\partial u'}{\partial x} + \rho_o v' \frac{\ell}{\delta} \frac{dM_o^*}{dy} + \frac{1}{\gamma} \frac{\partial p'}{\partial x} = 0 \tag{2}$$

and

$$\rho_o M_o^* \frac{\partial v'}{\partial x} + \frac{1}{\gamma} \frac{\ell}{\delta} \frac{\partial p'}{\partial y} = 0 \tag{3}$$

for the momentum equations, and

$$p' + \frac{1}{2}\{(\gamma-1) M_o^{*2} - (\gamma+1)\} \rho' + (\gamma-1) M_o^* \rho_o u' = 0 \tag{4}$$

for the energy equation.

In these equations all flow quantities are non-dimensionalized by their critical (sonic) values; the subscript o and superscript ' denote basic flow and perturbation flow, respectively. Then, the non-dimensional velocity components are given by $M_o^* + u'$ and v' and the non-dimensionalized pressure, density by $p_o + p'$, $\rho_o + \rho'$, respectively. The x-coordinate is non-dimensionalized by ℓ and the y-coordinate by δ. γ is the ratio of specific heats. By introducing a function $\varphi(x,y)$, such that

$$p' = -\gamma \frac{\partial \varphi}{\partial x}, \quad v' = \frac{\ell}{\delta} \frac{1}{\rho_o M_o^*} \frac{\partial \varphi}{\partial y}, \tag{5}$$

we obtain for eqs. (1), (2), (3) the single equation

$$\left(\frac{\ell}{\delta}\right)^2 \varphi_{yy} - (M_o^2-1)\,\varphi_{xx} - \left(\frac{\ell}{\delta}\right)^2 \frac{2}{M_o}\frac{dM_o}{dy}\,\varphi_y = 0 \qquad (6)$$

where $M_o(y) = M_o^*(y)\sqrt{\rho_o(y)}$ [1] and the partial derivatives are denoted by subscripts.

Eq. (6) is integrated between $x = \pm L$ and the boundary conditions are (Fig. 2):

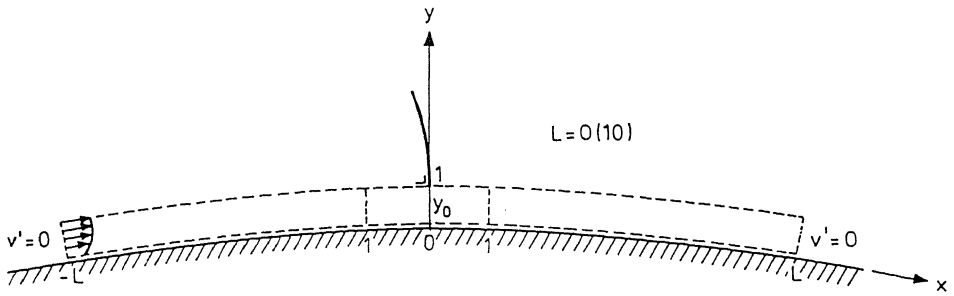

Fig. 2 : Region of integration.

1. at $x = \pm L$, $v' = 0$, giving

$$\varphi_y(-L,y) = \varphi_y(L,y) = 0 \qquad (7)$$

2. at the outer edge of the inviscid upper layer, $y = 1$, p' is prescribed by the external flow, thus

$$\varphi_x(x,1) = -\frac{1}{\gamma}\,p'(x,1) \qquad (8)$$

3. at the inner edge, $y = \frac{\delta_\mu}{\delta} = y_o$, we have $p'_y(x,y_o) = 0$, so that with eqs (3) and (7)

$$\varphi_y(x,y_o) = 0 \qquad (9)$$

The thickness y_o of the viscous sublayer is considered as the y position where the viscous and inviscid stresses balance; above y_o the inertia stresses are dominant, below y_o the viscous stresses are dominant.

According to [1] the x derivative of the wall shear stress τ_w is taken as the characteristic physical quantity of which the parametric dependance of y_o is analysed; this derivative is expressed as

$$\frac{1}{a^*}\frac{\partial \tau_w}{\partial x} = \mu \frac{\partial^2 u'(x, o; y_o)}{\partial x \, \partial y} \tag{10}$$

where a^* is the critical speed of sound and μ the dynamic viscosity coefficient.

To evaluate eq. (10) the perturbation velocity u' is determined in the viscous sublayer by solving the perturbation equations in the sublayer [1] under the assumption that v' = 0. Then u' is found as an explicit function of x and y with y_o as a parameter. The particular thickness of the viscous sublayer is taken as that value of y_o for which $\frac{\partial \tau_w}{\partial x}$ shows a minimum with respect to y_o. That is, at the foot of the shock wave

$$\frac{\partial}{\partial y_o}\left(\frac{\partial^2 u'(o,o)}{\partial x \, \partial y}\right) = 0$$

In the numerical computation it was found that eq. (10) showed such a minimum for y_o of the order 10^{-2}. The perturbation pressure along the outer edge of the upper inviscid layer in front of the shock wave has been taken constant [1], namely

$$p'(x,1) = p'(-L,1) = \left[\frac{\gamma+1}{2+(\gamma-1)\, M^2(-L,1)}\right]^{\frac{\gamma}{\gamma-1}} - 1 \tag{11}$$

The pressure jump across the shock wave is then given by the normal shock relations.

For the pressure prescribed at the edge of the inviscid layer downstream of the incident shock the expressions of the Oswatitsch-Zierep theory [1,3] are applied. These expressions read

$$\hat{u}'(x,1) = \hat{u}'(o,1) - \frac{1}{\pi\sqrt{1-\hat{M}^2(o,1)}}\left[\frac{2\ell}{R_w} - \frac{\partial v'(o,1)}{\partial x}\right](2\, x\, \ell n\, x + x) + \tag{12}$$

and

$$-4\, s_{10}\, \hat{u}'(o,1)x$$

$$\hat{v}'(x,1) = -\left[\frac{\ell}{R_w} - \frac{\partial v'(o,1)}{\partial x}\right] x \tag{13}$$

where $\hat{}$ denotes quantities downstream of the shockwave, R_w is the radius of wall curvature and s_{10} is a free parameter matching the boundary layer flow to the external flow field. Integrating the momentum equation, eq. (2), with respect to x we obtain

$$\hat{p}'(x,1) = -\gamma\rho_o(1)\left[M_o^*(1)\{\hat{u}'(x,1)-\hat{u}'(o,1)\} + \frac{\ell}{\delta}\frac{dM_o^*(1)}{dy}\int_o^x \hat{v}'(\xi,1)d\xi\right]+\hat{p}'(o,1) \quad (14)$$

Since $\hat{p}'(x,1)$ is not known a priori, it requires a known flow in the inviscid upper layer (and vice versa, the determination of the flow field in the upper layer requires known values of $\hat{p}'$ at the edge of the layer); $\hat{p}'$ has to be determined iteratively.

3. Numerical solution

Computational method

The boundary value problem given by eqs (6)-(9) together with eq. (14) has been solved numerically by a standard finite element method, consisting of a package of FORTRAN subroutines. The package, called AFEP (A Finite Element Package), is described in detail in [4]-[6].
In the present application the computational domain is subdivided in a number of subdomains, shown in Fig. 3, where each pair of numbers represents the sub-boundary and the number of meshpoints, respectively. The total number of meshpoints is 1121.

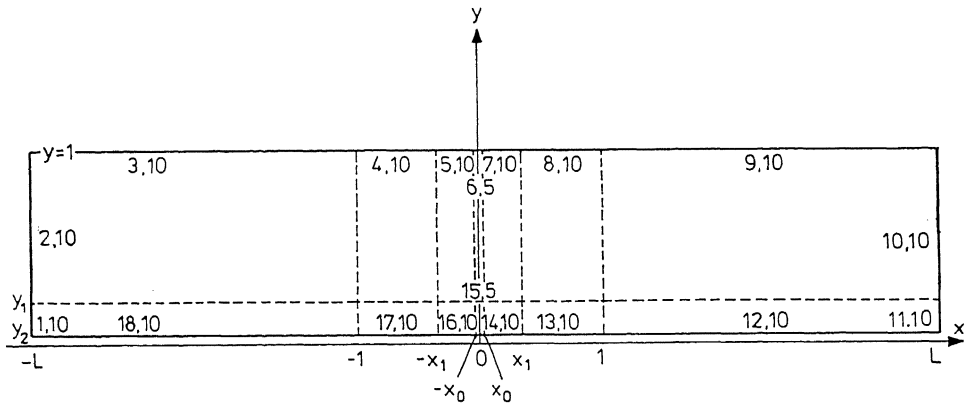

Fig. 3 : Distribution of meshpoints in the computational program.

The shock wave et the outer edge of the inviscid upper layer is confined within the interval $[-x_o,x_o]$, where $x_o=10^{-6}$, then the numerical pressure rise is almost discontinuous. In regions where the derivatives of flow quantities are large a fine meshwidth has been chosen. The streamwise dimension of the computational domain is taken as L = 10.

The computational domain is now divided into triangular elements, the corner points of which are the above mentioned meshpoints.

Initial velocity profile

As incoming velocity profile at x = -L a turbulent boundary layer profile has been taken, given by

$$M_o^*(y) = M_o^*(1)\left[1 + \frac{1}{K}\left\{\frac{c_f(-L)}{2}\left(1 + r\,\frac{\gamma-1}{2}\,M^2(-L,1)\right)\right\}^{\frac{1}{2}}\{\ln y - 0.5(1+\cos\pi y)\}\right] \quad (15)$$

where $M_o^*(1) = 1$ [1], the von Kármán constant $K = 0.41$, $c_f(-L)$ is the skinfriction coefficient at x = -L, the recovery factor for a turbulent boundary layer $r = 0.89$ and $M(-L,1)$ is the Mach number of the flow at the edge of the boundary layer at x = -L. The term $\ln y$ describes the logarithmic law of the wall of the velocity profile; $(1+\cos\pi y)$ is the additional term of the Coles wake function, it is multiplied by 0.5 in the case of a turbulent boundary layer with zero pressure gradient.

Boundary conditions along upper and lower boundaries of the inviscid layer

The determination of the thickness y_o of the viscous sublayer is part of the solution procedure of the flow problem in the inviscid upper layer. Since $y_o = O(0.01)$ [1], as an initial guess y_o is assumed to belong to the interval $0.005 \leq y_o \leq 0.015$. Then, for three distinct values of y_o, displayed regularly in that interval, the boundary value problem is solved, yielding the u' and p' distributions along the edge of the sublayer. Using eq. (10), we may now compute $\frac{\partial \tau_w}{\partial x}(o,o)$ for each of the distinct values of y_o. Fitting a parabola through the results for these three values, a minimum value of $\frac{\partial \tau_w}{\partial x}(o,o)$ may be found at $y_o = (y_o)_{min}$. Of course $(y_o)_{min}$ should ly within the aforementioned interval, if this is not the case the procedure should be repeated for a new interval of y_o. Depending on the particular problem, values between 0.013 and 0.014 were obtained. The perturbation pressure at the outer edge is computed according to eqs (11)-(14) and using the normal shock relations. Downstream of the shock wave and behind the minimum in the after-expansion region a linear pressure distribution is applied until at x = L the pressure recovery is 90% of its value just across the shock wave.

The pressure applied at the outer edge of the inviscid layer downstream of the shock requires a known flow field of the inviscid upper layer. Therefore this flow problem has also been treated iteratively; the first iteration sweep has been performed for a constant pressure, being the value just across the shock wave which is obtained from eq. (11) using normal shock relations.
The free parameter s_{10} in eq. (12) has been taken such as to give a good matching with the inviscid outer flow field. In fact the results of experiments in [2] and [7] have been used.

Computation of perturbation pressure and velocity

In all meshpoints of the inviscid upper layer p' and v' are determined from eq. (5) using the standard subroutines of the AFEP package. Eq. (2) is integrated with respect to x, knowing the incoming velocity profile at x = -L, eq. (15), this yields u'.
The perturbation pressure in the viscous sublayer is obtained from the results in the inviscid upper layer for an established value of y_o, giving $p'=p'(x,y_o)$ since $\frac{\partial p'}{\partial y}$ in the sublayer is assumed to be zero [1].

4. Results

The numerical results are compared to some experimental data [2] for a convex surface (R ≈ 0.5 m) and to those [7] for a plane wall. The comparison has been made for different Mach numbers M at the edge of the boundary layer just ahead of the shock wave, and for different Reynolds numbers Re. The Reynolds number is based on the length of the convex plate [2] or on the length of the plane wall on which the boundary layer develops [7]. Also other theoretical results have been compared to those measurements [1], [8]-[11]. The results of Messiter [9] are only available downstream of the shock.

All numerical surface pressure distributions show a steeper pressure rise than the experimental distributions (Figs 4-6).

It should be mentioned that the theoretical pressures of Inger and Mason [10] and of Melnik and Grossman [11], Fig. 6, are in better agreement with the initial pressure rise than the results obtained by the Bohning-Zierep model.

This is probably due to the better model description in [10] and [11] which is closer to the real viscous flow behaviour, whereas in the Bohning-Zierep model used in [1,8] and in the present method the sublayer is very thin indeed, about 1% of the boundary layer thickness.

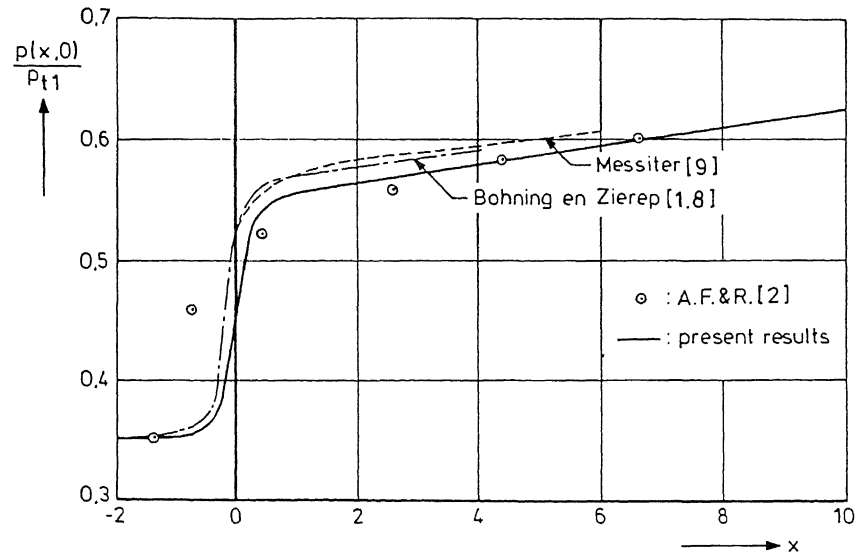

Fig. 4: Surface pressure distribution: M=1.3225, Re = 2.63·10^6

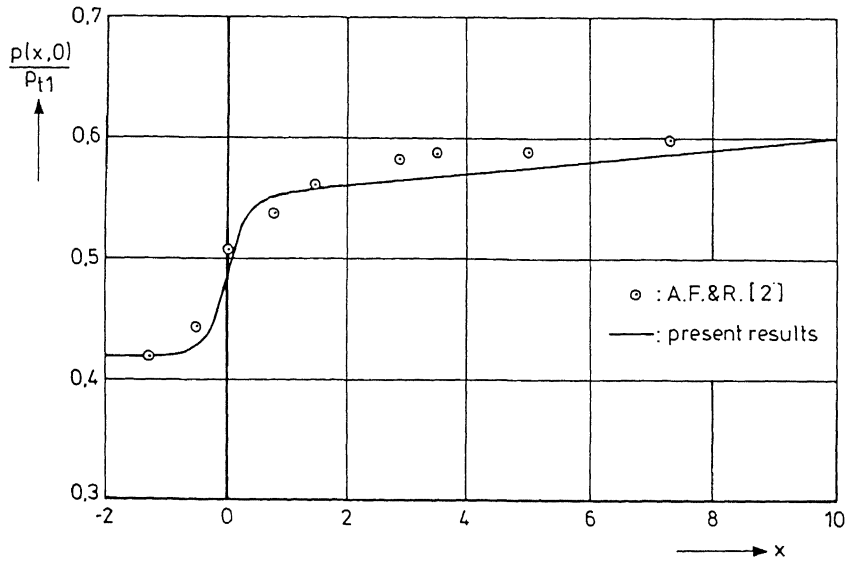

Fig. 5: Surface pressure distribution: M=1.1897, Re = 2.658·10^6

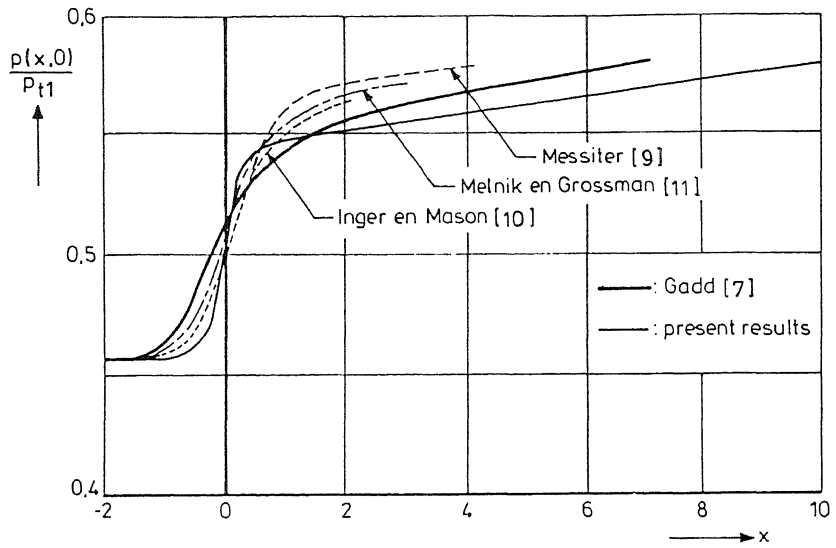

Fig. 6: Surface pressure distribution: M = 1.12, Re = $6.0 \cdot 10^6$

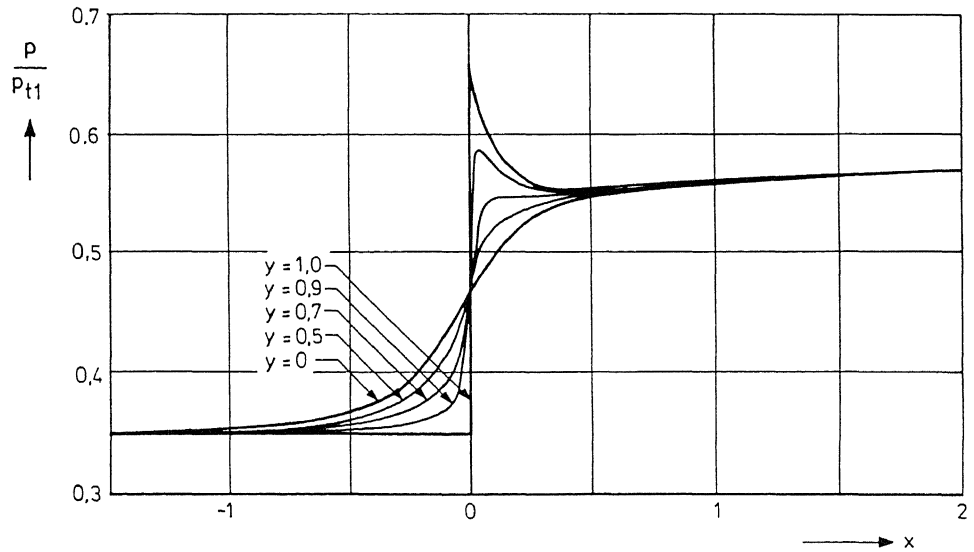

Fig. 7: Pressure distribution in the boundary layer : M = 1.3225, Re = $2.63 \cdot 10^6$

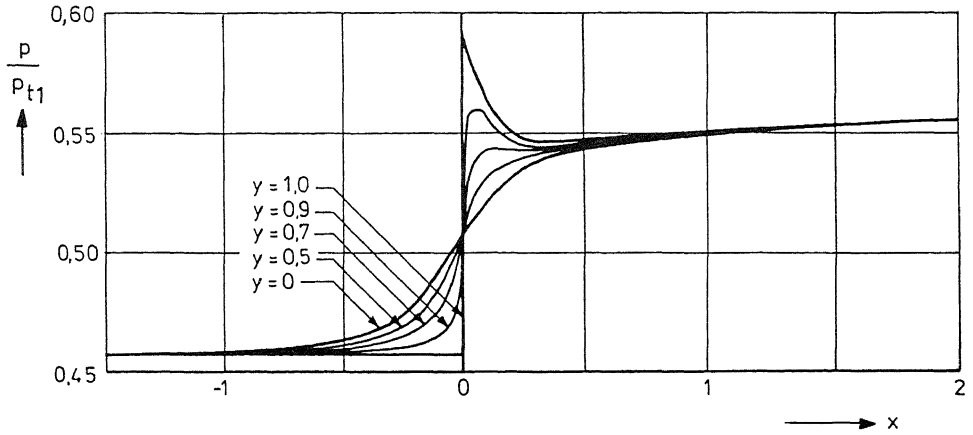

Fig.8: Pressure distribution in the boundary layer: M=1.12, Re = $6.0 \cdot 10^6$.

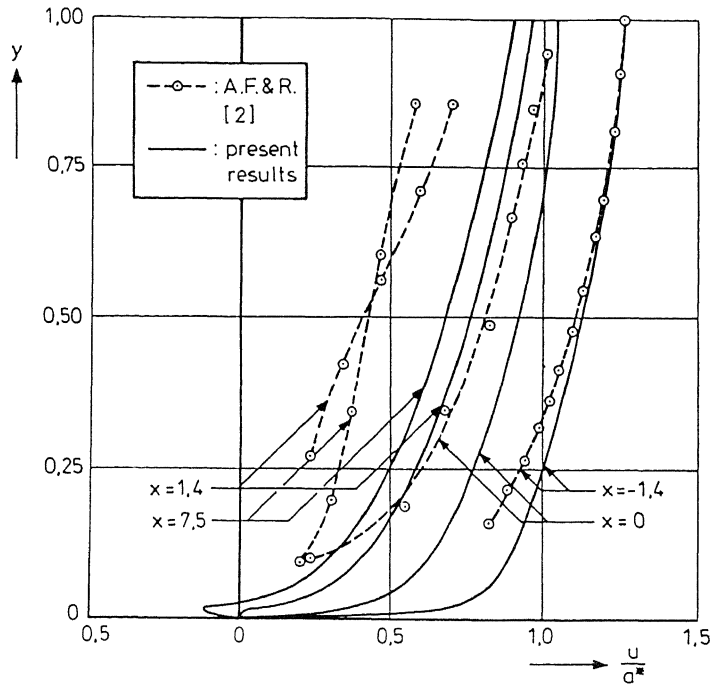

Fig.9: Velocity profiles : M = 1.3225, Re = $2.63 \cdot 10^6$.

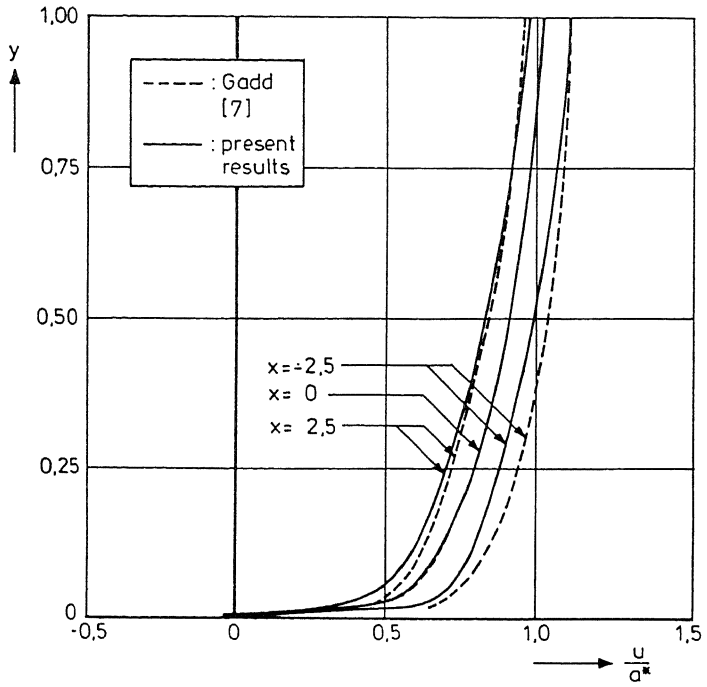

Fig.10: Velocity profiles : M=1.12, Re = $6.0 \cdot 10^6$.

Figs 7 and 8 represent the diffusion towards the wall of the steep pressure jump applied at the edge of the layer.

The velocity profiles are plotted in Figs 9 and 10. There exists a substantial disagreement between theory and experiment for the higher Mach number case (Fig. 9). This may be expected since the Bohning-Zierep model is based on the disturbance of a M = 1 basic flow, therefore a better agreement results for a Mach number closer to unity (Fig. 10).

Another reason for the disagreement in the case of Fig. 9 may be the difficulty of having a correct incoming velocity profile at x = -L, since in the experiments of [2] there is no profile given at that position. The numerical results show a reverse flow in the case of Fig. 9. Since the flow model does not cover such a phenomenon, this result should be considered with some doubt; it might only indicate the breakdown of the flow model and one has to look for a different approach, as has been down in [12].

From Fig. 11, where the distribution of the vertical velocity component is shown, it may be seen that the upwash in the inviscid upper layer accumulated into a discontinuity at the foot of the shock wave, indicating an oblique shock wave and a kinked streamline.

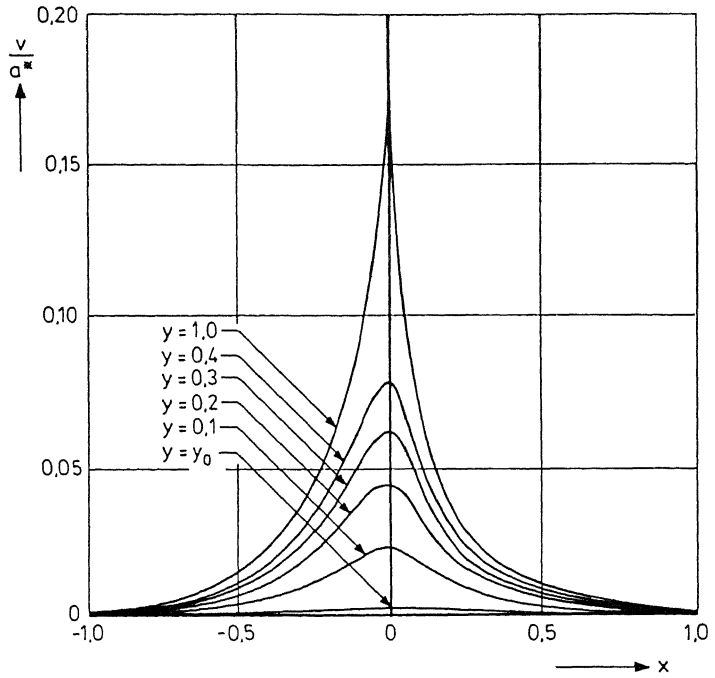

Fig.11: Vertical velocity component: M=1.3225, Re= $2.63 \cdot 10^6$

In the initial boundary conditions the pressure jump across the shock wave was obtained by normal shock relations, thus involving no vertical velocity component. An oblique shock does not have a singularity at its foot on a curved surface. There is, however, always the possibility of an after-expension that is regular in the sense that the streamline is convex downstream of the shock, as shows the v-distribution in Fig. 11.

The v-distribution is asymmetric with respect to x = 0. At $y = y_o$, the edge of the viscous sublayer, v should vanish as the boundary condition states. In the AFEP computation procedure the Neumann conditions are satisfied better if the meshsize in vertical direction is decreased in the vicinity of the boundary. In the present computercode we have not tried the utmost.

5. Concluding remarks

The implementation of the Bohning-Zierep model [1] into a numerical method of the shock wave - boundary layer interaction problem delivers a more universal treatment of the flow problem than the analytical method given in [1] because

of the larger applicable variety of flow parameters.
As is the case with most of the existing numerical methods the agreement among themselves is better than the agreement with experimental results. This may be due to the insufficient modelling of viscosity and, certainly, of turbulence.
In the flow model introduced in [1], which is applied numerically in the present paper, the initial normal shock changes into an oblique one as the numerical procedure iterates to the final solution. As a consequence the Oswatitsch-Zierep singularity [3] at the foot of the shock vanishes and so does the accompanying after-expansion belonging to a normal shock at a convex wall. However, also oblique shocks inpinging on a boundary layer are succeeded by expansion regions. Therefore, instead of having a normal shock, it would be interesting to apply as incident shock on the edge of the inviscid upper layer a shock wave which is slightly oblique and which is followed by an expansion region. A comparison of the results obtained with the present numerical method and using the two different boundary conditions, might be helpful in the discussion [13] which of the two conditions is most likely. Such an extension of the flow model will be the subject of future work at the Laboratory for High Speed Aerodynamics of the Department of Aerospace Engineering.

6. References

1. Bohning, R. and J. Zierep, 'Der senkrechte Verdichtungsstoss an der gekrümmten Wand unter Berücksichtigung der Reibung', ZAMP 27 (1976), p. 225-240.
2. Ackeret, J., F. Feldmann and N. Rott, 'Untersuchungen an Verdichtungsstössen und Grenzschichten in schnell bewegten Gasen', Mitteilungen aus dem Institut für Aerodynamik and der E.T.H. Zürich, Nr. 10, 1946.
3. Zierep, J., 'Theorie der Schallnahen und der Hyperschallströmungen', Verlag G. Braun, Karlsruhe, 1966.
4. Segal, A., 'AFEP User Manual', Dept. of Mathematics and Informatics, Delft University of Technology, Delft, 1981.
5. Segal, A., 'AFEP Standard Elements', Dept. of Mathematics and Informatics, Delft University of Technology, Delft, 1981.
6. Segal, A., 'AFEP Programmers Guide', Dept. of Mathematics and Informatics, Delft University of Technology, Delft, 1981.
7. Gadd, G.E., 'Interactions Between Normal Shock Waves and Turbulent Boundary Layers', Aeronautical Research Council, London, R&M 3262, 1962.

8. Bohning, R. and J. Zierep, 'Normal Shock - Turbulent Boundary Layer Interaction at a Curved Wall', AGARD-CP-291, 1980.
9. Messiter, A.F., 'Interaction Between a Normal Shock Wave and a Turbulent Boundary Layer at High Transonic Speeds, Part I: Pressure Distribution, ZAMP 31 (1980), p. 204-226.
10. Inger, G.R. and W.H. Mason, 'Analytical Theory of Transonic Normal Shock Turbulent Boundary Layer Interaction', AIAA Journal Vol. 14 (1976), p. 1266-1272.
11. Melnik, R.E. and B. Grossman, 'Analysis of the Interaction of a Weak Normal Shock Wave with a Turbulent Boundary Layer', AIAA Paper, No. 74-598, 1974.
12. Bohning, R. and J. Zierep, 'Bedingung für das Einsetzen der Ablösung der turbulenten Grenzschicht an der gekrümmten Wand mit senkrechtem Verdichtungsstoss', ZAMP 29 (1978), p. 190-198.
13. Inger, G.R., 'Transonic Shock-Turbulent Boundary Layer Interaction and Incipient Separation on Curved Surfaces', AIAA Paper, No. 81-1244, 1981.